IEICE TRANS. ELECTRON., VOL. E76-C, NO. 2 FEBRUARY 1993

PAPER Special Issue on Optical/Microwave Interaction Devices, Circuits and Systems

Design of Ultrawide-Band, High-Sensitivity p-i-n Protodetectors

Kazutoshi KATO†, Susumu HATA†, Kenji KAWANO† *and* Atsuo KOZEN†, *Members*

SUMMARY We show the design of the bandwidth and the external quantum efficiency (including the coupling efficiency to a single-mode fiber) of p-i-n photodetectors. Based on their design procedures, the performance limits of both conventional surface-illuminated photodetectors and side-illuminated photodetectors are evaluated. We point out that in the ultrawide-band region, optical waveguide photodetectors have great advantages over conventional surface-illuminated photodetectors in terms of the product of the bandwidth and the external quantum efficiency. It is shown that a 100-GHz bandwidth can be achieved with little degradation of the external quantum efficiency by a multimode waveguide photodetector structure. We also present a design concept for overcoming the performance limits of solitary waveguide photodetectors by including an input tapered optical waveguide.

key words: p-i-n photodetector, semiconductor, microwave, multimode waveguide

1. Introduction

Highly efficient photodetectors with a broad bandwidth will be key components of future wide-band optical communication systems. It is well known that wide-band operation equates to a small device capacitance and a short carriertransit time. However, for a small capacitance, the device itself must be small, which may lead to coupling losses with the input optical beam. On the other hand, a short transit time generally requires the photo-absorption layer to be very thin, resulting in degradation of the internal quantum efficiency (η_{int}). As a result, these requirements tend to work against the achievement of high sensitivity. A theoretical analysis[1] has revealed that the product of the bandwidth (the 3-dB electrical frequency) f_{3dB} and η_{int} of conventional surface-illuminated photodetectors cannot exceed a few tens of gigaherz in the ultrawide-band region.

To overcome this adverse tradeoff between the electrical and optical properties, side-illuminated optical waveguide photodetectors (WGPDs) have received a great deal of interest[1]–[5] because their structure permits f_{3dB} and η_{int} to be specified almost independently of each other. In these devices, the core layer of the waveguide acts as a photo-absorption layer. However, the chief drawback of WGPDs is that they are difficult to couple to single-mode fibers with high efficiency, and as a result, their full potential has not been realized yet.

In this paper, we present a theoretical analysis of photodetector performance, such as their bandwidth and quantum efficiency. On the basis of these numerical results, we demonstrate the superiority of WGPDs over conventional surface-illuminated photodetectors, and propose a new type of WGPD which has a multimode waveguide configuration in order to achieve a high coupling efficiency to the input optical fiber. For such multimode waveguide photodetectors, the design concepts involved in achieving both ultrawide-band operation and a high external quantum efficiency are also presented. Our experimental results verify these concepts, and we have made a photodetector with a bandwidth of 50 GHz and an external quantum efficiency of 68%. We also introduce a WGPD design which involves integrating a WGPD with an input tapered optical waveguide, which enables the performance limits of solitary WGPDs to be overcome.

2. Photodetector Properties

2. 1 Bandwidth

The bandwidth of a photodetector is limited by both the carrier-transit time and the CR-time constant. Assuming these limiting factors are independent of each other and have Gaussian responses, the f_{3B} of the photodetector can be approximated as[6]

$$\frac{1}{f_{3dB}^2}=\frac{1}{f_t^2}+\frac{1}{f_{CR}^2} \tag{1}$$

where f_t is the 3-dB electrical frequency when the CR-time constant is very small, and f_{CR} is the 3-dB electrical frequency when the carrier-transit time is very small. We will demonstrate the validity of the above approximation at the end of this section. For ultrawide-band operation, it is necessary to improve both of these parameters.

Let us start with a few general observations about the transit time of photogenerated carriers in a photodetector. Light impinging on a depleted photo-absorption layer generates an electron and a hole, which are drawn to the n-type and p-type layers,

Manuscript received August 25, 1992.

† The authors are with NTT Opto-electronics Laboratories, Atsugi-shi, 243-01 Japan.

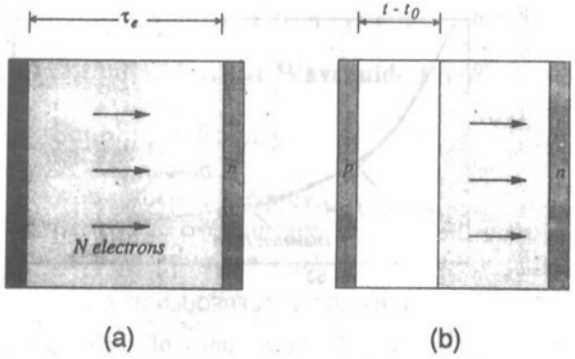

Fig. 1 Electron distribution in the photodetector at (a) t_0 and (b) t.

respectively. To simplify this model we will focus only on the electron behavior. Assuming the light uniformly illuminates a photo-absorption layer of thickness D and that each electron travels at the saturation velocity v_e, at time t the number of the electrons N generated at time t_0 is reduced to $N\{1-(t-t_0)/\tau_e\}$ as shown in Fig. 1, where τ_e is D/v_e (electron transit time through the depleted photo-absorption layer). Although an exact result can be obtained by taking into account the distribution of light illumination as previously studied,[1],[7] the above assumption produces a good approximation, especially when we calculate the efficiency of wide-band photodetectors and WGPDs. When the intensity of the light is modulated by a function $\exp(j\omega(t-t_0))$, the current generated by the photodetector is

$$N\left(1-\frac{t-t_0}{\tau_e}\right)\frac{q}{\tau_e}\exp(j\omega(t-t_0)) \tag{2}$$

where q is the elementary charge. The electrons that are generated after $t-\tau_e$ exist at time t in the photo-absorption layer. Thus, we can obtain the normalized overall current at time t by integrating Eq. (2) from $t-\tau_e$ to t, and modifying it to include the contribution of the holes:

$$\frac{I(\omega)}{I(0)}=\left[\frac{1}{\omega^2\tau_e^2}\{1-\exp(j\omega\tau_e)\}-\frac{1}{j\omega\tau_e}\right]+\left[\frac{1}{\omega^2\tau_h^2}\{1-\exp(j\omega\tau_h)\}-\frac{1}{j\omega\tau_h}\right]. \tag{3}$$

f_t is defined as the frequency at which Eq. (3) is equal to $1/\sqrt{2}$, and can be calculated as

$$f_t\cong\frac{3.5\ \bar{v}}{2\pi D} \tag{4}$$

where $\bar{v}$ is defined as

$$\frac{1}{\bar{v}^4}=\frac{1}{2}\left(\frac{1}{v_e^4}+\frac{1}{v_h^4}\right). \tag{5}$$

The above expressions produce a good approximation with an error of a few percent, and thus suitable for qualitative estimation. Figure 2 shows the normalized microwave power responses calculated from Eq. (3) where it is assumed that $v_e=6.5\times10^6$ cm/s and $v_h=4.8\times10^6$ cm/s.[1] At a thickness of around 0.4 μm—the usual core layer thickness of semiconductor optical waveguides—f_t changes significantly and has an inverse relationship to D as described by Eq. (4).

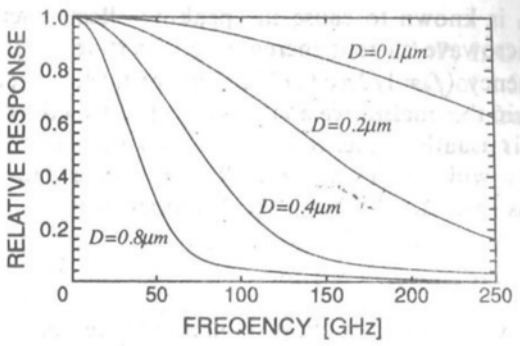

Fig. 2 Calculated microwave power response.

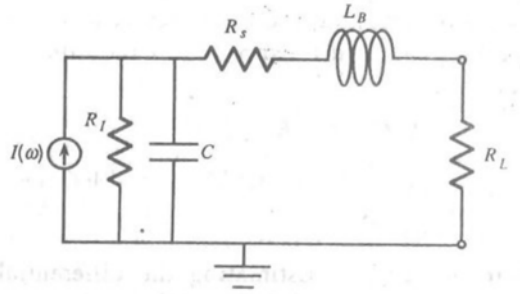

Fig. 3 Photodetector equivalent circuit.

Next, consider the CR-time constant of the circuit. Although SPICE simulation is usually a powerful technique for predicting circuit performance quantitatively, an analytical approach is useful in designing photodetectors. As shown in the equivalent circuit of Fig. 3, a photodetector is basically a current source with a capacitance of C and an internal resistance R_I, where R_L, R_S, and L_B are a load resistance, a stray resistance, and an external inductance, respectively. C is determined by D and the area of the photo-absorption layer S:

$$C=\frac{\varepsilon_0\varepsilon_r S}{D} \tag{6}$$

where $\varepsilon_0\varepsilon_r$ is the dielectric constant of the photo-absorption layer. Assuming the dark current of the photodetector is very low—less than a few micro-amperes—R_I becomes very high compared with the other elements and can be omitted from the equivalent circuit. The microwave current which flows through R_L then becomes

$$\frac{I(\omega)}{I(0)}=\frac{1}{1-\omega^2L_BC+j\omega C(R_L+R_S)} \tag{7}$$

L_B is known to cause the peaking effect whereby the microwave current increases at a certain resonant frequency ($f_r=1/2\pi\sqrt{L_BC}$). This effect has been ignored in the qualitative analysis at pervious works because f_r is usually higher than f_{3dB} and does not influence f_{3dB} in a wide-band—around 10 GHz—photodetector. In this case, the 3-dB electrical frequency is

$$f_{CRO}=\frac{1}{2\pi C(R_L+R_S)} \tag{8}$$

However, in an ultrawide-band—higher than 30 GHz—photodetector, L_B can actually help to push up the speed.[8] The following discussion includes the contribution made by L_B in the estimation of f_{CR}.

f_{CR} is defined as the frequency at which Eq. (7) is equal to $1/\sqrt{2}$, and is expressed by the following equation:

$$\omega'=\{(2L_BC-C^2(R_L+R_S)^2 +\sqrt{8L_B^2C^2-4L_BC^3(R_L+R_S)^2+C^4(R_L+R_S)^4}) /2L_B^2C^2\}^{1/2} \tag{9}$$

where $\omega'=2\pi f_{CR}$. Estimating the differential of the right part of Eq. (9), it is found that ω' has a maximum of $\sqrt{2}/C(R_L+R_S)$ at $L_B=C(R_L+R_S)^2/2$. Consequently, the optimum f_{CR} is given by

$$f_{CR}=\frac{\sqrt{2}}{2\pi C(R_L+R_S)}=\sqrt{2}f_{CRO}. \tag{10}$$

Equation (10) means that the 3-dB electrical frequency can be increased by 40% by adjusting L_B. This feature plays a significant part in the design of photodetectors. From Eqs. (4), (6), and (10), it is easily deduced that f_{CR} is proportional to D and that maximizing f_{3dB} in Eq. (1) involves a tradeoff between f_t and f_{CR}.

We should also consider the validity of Eq. (1). Since neither the microwave current characterized by the carrier-transit time (Eq. (3)) nor that by the CR-time constant (Eq. (7)) have Gaussian responses. Thus, if we want to get an exact value for f_{3dB}, we should calculate the total frequency response from the product of Eqs. (3) and (7). By calculating the exact value of f_{3dB} and comparing it with the approximate value obtained using Eqs. (1), (4), and (10), we confirmed that Eq. (1) provides a good approximation with an error of less than 5%.

2.2 Quantum Efficiency

The external quantum efficiency η_{ex} is given by

$$\eta_{ex}\cong(1-R)\,\eta_c\eta_{int} \tag{11}$$

where R, η_c, and η_{int} are the power reflection loss at the facet of the photodetector, the fiber coupling efficiency, and the internal quantum efficiency, respectively. The internal quantum efficiency η_{int} is given by

$$\eta_{int}\cong 1-\exp(-\Gamma\alpha d) \tag{12}$$

where Γ, α, and d are the confinement factor, the absorption coefficient, and the length in the direction parallel to the beam, respectively, for the photo-absorption layer. The value of α is about $(1.5\ \mu m)^{-1}$ for a 1.55-μm-wavelength photodetector. Thus, for a conventional surface-illuminated photodetector—for which Γ is unity—a photo-absorption layer thicker than 1.5 μm is generally required for high efficiency even though it degrades f_t.

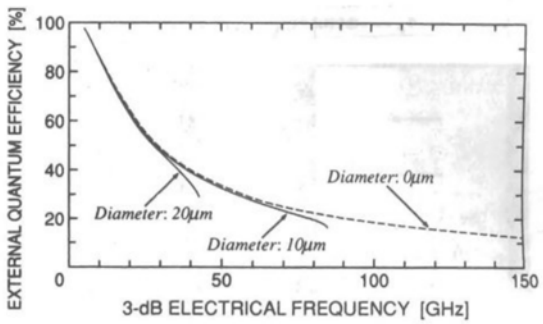

Fig. 4 Theoretical performance limits of surface-illuminated photodetectors.

We are now in position to estimate the performance limit of the surface-illuminated photodetector based on Eqs. (1), (4), (10), and (11). Assuming η_c is unity—the essential difference from WGPDs—and R is zero, η_{ex} is equal to η_{int}. Figure 4 shows the external quantum efficiency of photodetectors which is designed to have a 3-dB electrical frequency indicated by the horizontal axis. Solid curves represent photodetectors with diameters of 10 and 20 μm. Both curves and at the maximum bandwidth determined by the tradeoff between f_t and f_{CR} shown in Eq. (1). The dotted curve indicates the performance of a photodetector with an infinitely small diameter. We can see from these results that the product $f_{3dB}\eta_{ex}$ is about 20 GHz in the ultrawide-band region, and that ultrawide-band operation above 100 GHz is difficult—because the diameter should in practice be at least 5 μm—even if we give up trying to achieve a high η_{ex}.

For a side-illuminated WGPD, on the other hand, d does not correspond to the thickness of the photo-absorption layer D but is identical to the length of the device L, so that f_t and η_{int} can be specified almost independently of each other. In this type of photodetector, because the photo-absorption layer also acts as a waveguide core layer, Γ decreases with decreasing D. Thus, from Eqs. (4) and (12), we can see that there is only a weak tradeoff between f_t and η_{int}.

3. Multimode Optical Waveguide Photodetector

3. 1 Coupling Efficiency

As described in the previous section, WGPDs have a big advantage over surface-illuminated types in that their $f_t\eta_{int}$ product is much higher. In a typical double-hetero InP/InGaAs/InP WGPD, the thickness of the InGaAs photo-absorption layer D determines not only f_t, f_{CR}, and η_{int} but also the coupling efficiency in the y direction η_{cy}—where $\eta_c=\eta_{cx}\eta_{cy}$ (x and y indicate directions parallel and perpendicular to the substrate surface, respectively). For example, for a device to operate at 50 GHz, D must be less than 0.6 μm to satisfy the carrier transit time as shown in Fig. 2. However, in WGPDs with such thin core layers, a spot size (half width at $1/e$ of maximum optical field) of the guided light is less than 0.5 μm, while a lens or a hemispherically-ended single-mode fiber focuses the light to a spot size greater than 1 μm. This substantial mismatch between the optical field distributions reduces the coupling efficiency and, as a result, the external quantum efficiency η_{ex} is greatly reduced.

To avoid this rigid tradeoff relationship, we tried to enlarge the optical field distribution of the WGPDs by adding doped InGaAsP layers between the InGaAs layer and the InP layers.[9] Since the bandgap energy of the InGaAsP layers correspond to a 1.3 μm wavelength, photo-carriers are generated and transported only in the depleted InGaAs layer. With this arrangement, f_t is still determined only by the thickness of the InGaAs layer, while the optical properties are improved. Two WGPD models were developed, one with a symmetric structure and the other with an asymmetric structure, as shown in Figs. 5(a) and (b), respectively. We assumed both WGPDs to have a high-mesa structure.

First, the optical fields of the guided light in the WGPD structures were calculated using the step segment method (SSM).[10],[11] We assumed that the optical fields of lossy waveguides such as WGPDs could be calculated by ignoring the imaginary part of the refractive indices. We thus selected values of 3.17, 3.39, and 3.59 for the refractive indices of InP, InGaAsP, and InGaAs, respectively, at a wavelength of 1.55 μm. The numerical results displayed the following features:
(1) When the total thickness of the InGaAs and InGaAsP layers is less than 1.1 μm, only the fundamental ($j=0$) mode, or the fundamental and first order ($j=1$) modes exist. On the other hand, when the total thickness is above 1.1 μm, higher-order ($j>1$) modes appear.
(2) The optical field distributions of the TE and TM modes are almost the same.
(3) The above features can be seen in both the symmetric and asymmetric structures.
(4) Those features depend not on the thickness of the InGaAs layer, but on the total thickness.

We will refer to the WGPDs with several even order modes—those with a total thickness of more than 1.1 μm—as *multimode* WGPDs.

Next, we calculated the coupling efficiency in the y direction η_{cy} by considering the overlap integral between the optical field of the fiber and that of the WGPD. Figure 6 shows the coupling efficiency between a hemispherically-ended single-mode fiber which produces a Gaussian beam with spot size of 1.3 μm and WGPDs with a 0.6-μm InGaAs layer as a function of the total thickness of the InGaAs and InGaAsP layers. For both the symmetric and asymmetric structures, when the total thickness slightly exceeds 1.1 μm, giving the WGPD a multimode configuration, η_{cy} increases dramatically to as much as 90%. This is because the additional coupling efficiency attributable to the higher-order modes $\eta_{cyj}(j>1)$ contributes to $\eta_{cy}(=\sum_j \eta_{cyj})$.

The total optical field distribution of a multimode WGPD in the y direction $\Phi(y)$ can be obtained by summing up the field distribution for each mode:

$$\Phi(y)=\sum_j C_{yj}\phi_{yj}(y) \tag{13}$$

where $|C_{yj}|^2=\eta_{cyj}$ and ϕ_{yj} is the normalized wavefunction of the jth-order mode in the y direction. Figure 7 shows the calculated total field distributions of symmetric structures with (a) a total thickness of 0.6 μm, (b) a total thickness of 1.4 μm, and (c) a total thick-

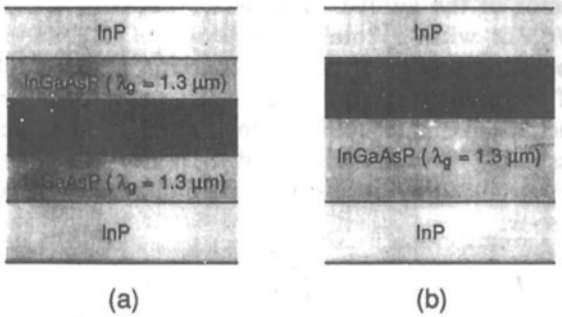

Fig. 5 WGPD structure model, (a) symmetric, (b) asymmetric.

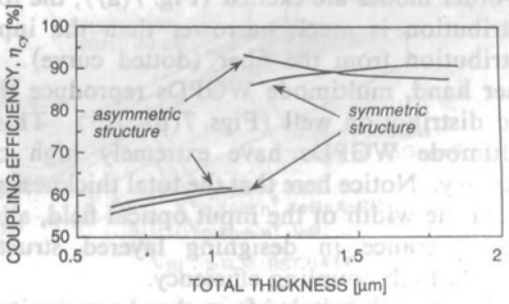

Fig. 6 Calculated coupling efficiency between a WGPD and a hemispherically-ended single-mode fiber.

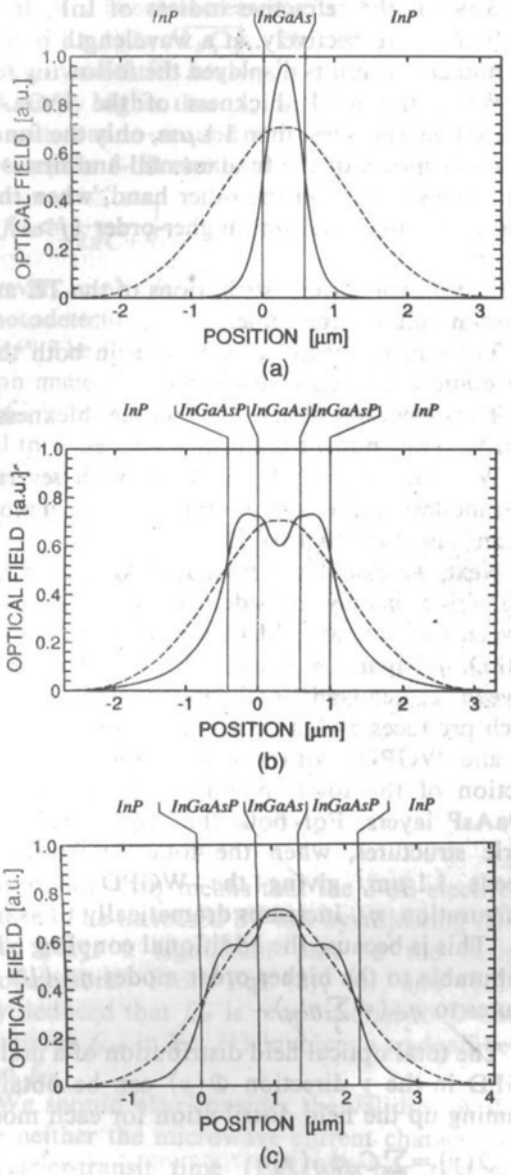

Fig. 7 Total field distribution of the guided light in the WGPD (solid curve) and input field distribution from the fiber (dotted curve). (a) total thickness 0.6 μm, (b) total thickness 1.4 μm, (c) total thickness 2.2 μm.

ness of 2.2 μm. When only the fundamental and 1st-order modes are excited (Fig. 7(a)), the total field distribution is much narrower than the input field distribution from the fiber (dotted curve). On the other hand, multimode WGPDs reproduce the input field distribution well (Figs. 7(b), (c)). This is why multimode WGPDs have extremely high coupling efficiency. Notice here that the total thickness need not exceed the width of the input optical field, allowing a great tolerance in designing layered structures to obtain a high coupling efficiency.

It can be concluded from the above results that the electrical and optical properties in the y direction can be designed almost independently of each other for multimode WGPDs.

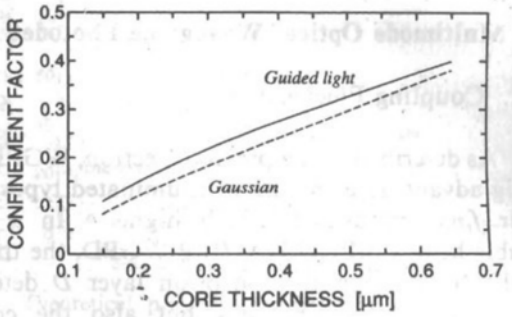

Fig. 8 Calculated confinement factor of the guided light (solid curve) and approximation based on the assumption that the distribution of the guided light is equal to the distribution of the input light (dotted curve).

3.2 The $f_{3dB}\eta_{ex}$ Limit

We designed multimode WGPDs with optimized electrical and optical properties using Eqs. (1), (4), (10), (11), and (12). Among the parameters in these equations, we have not yet discussed the confinement factor Γ of multimode WGPDs. Γ is given by

$$\Gamma=\Gamma_x\Gamma_y \tag{14}$$

where Γ_x and Γ_y are the confinement factors in the x and y directions. Since we assumed the WGPD to have a high-mesa structure in which the guided light is well confined in the x direction, Γ_x is unity. Γ_y is the integral of the total power distribution over the photo-absorption layer (core layer):

$$\Gamma_y=\int_{core}|\Phi(y)|^2dy. \tag{15}$$

Here a rough estimate of the confinemdnt factor is needed for outlining the performance limit.

However, it is difficult to calculate Γ_y exactly because the profile of the total field distribution depends on the photodetector layer structure as shown in Figs. 7(b) and (c). We found that Γ_y can be roughly estimated by assuming the total field distribution to be the same as the input field distribution. The solid curve in Fig. 8 shows the calculated confinement factor of the guided light in a symmetric multimode WGPD with a total thicknesses of 2.2 μm—corresponding to Fig. 7(c)—as a function of the thickness of the photo-absorption layer D. The dotted curve is the approximate confinement factor Γ_y' obtained by assuming that the total field distribution is equal to the input field distribution (a Gaussian beam with a spot size w:

$$\Gamma_y'=\int_{core}\left|\left(\sqrt{\frac{2}{\pi}}\frac{1}{x}\right)^{1/2}e^{-\frac{(y-y_0)^2}{w^2}}\right|^2dy \tag{16}$$

were y_0 is the center of the total field distribution of the

multimode WGPD. These curves are close to each other when D is larger than 0.2 μm—corresponding to an f_t of less than 150 GHz. These features are consistent with the fact that a multimode WGPD closely matches the input field distribution as described in the previous section. This result indicates that we can obtain a rough estimate of Γ_y with an error of less than 20% by calculating Γ_y'.

Based on the above results and discussions, the performance limit of a multimode WGPD was calculated in the following way:

(1) Starting with the spot size w of the input light as a parameter, the WGPD width was set at $2w$ so that an η_{cx} of more than 95% could be obtained.

(2) At a given f_{3dB}, we deduced the combinations of D and L which satisfy Eqs. (1), (4), (6), and (10).

(3) Using these paired values for D and L, we estimated η_{ex} using Eqs. (11), (12), and (16), and picked the pair which optimized η_{ex}.

The above procedure assumes that the photoabsorption layer is entirely depleted and the other layers are all undepleted, that the wavelength of the light is 1.55 μm, $v_e=6.5\times10^6$ cm/s, $v_h=4.8\times10^6$ cm/s, $\alpha=0.68$ μm^{-1},[1] $\varepsilon_r=13$, $R_L=50\,\Omega$, and that $\eta_{cy}=90\%$. To calculate the performance limits of the WGPD, we also assumed that $R_S=0\,\Omega$ and that $R=0$. Figure 9 shows the calculated $f_{3dB}\eta_{ex}$ limit of a multimode WGPD illuminated by Gaussian beams with spot sizes of 1, 2, and 3 μm. It can be seen that the input field distribution (or spot size) strongly affects the device performance. This is because a larger spot size requires a wider WGPD for which f_{CR} is smaller, which means that there is still a tradeoff between the electrical and optical properties in the x direction. Despite this fact, a comparison with the performance of the surface-illuminated photodetector shown in Fig. 4 shows that the WGPD has a great advantage at bandwidths above 10 GHz even when the spot size is 3 μm. Moreover, since a well-fabricated hemispherically-ended single-mode fiber can focus the light to a spot size of about 1 μm, it should be possible to realize a 100-GHz photodetector with little degradation of the external quantum efficiency. However, the parasitic elements and uncontrollable inductance will degrade this performance, and limiting these factors is the key in reaching the ideal performance shown in Fig. 9.

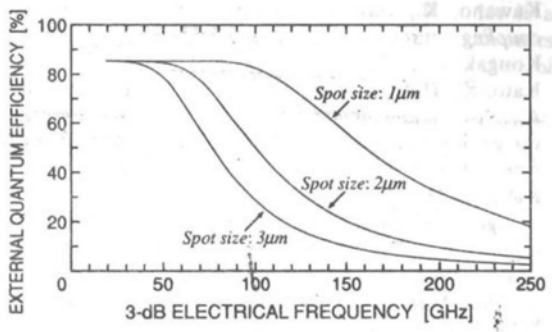

Fig. 9 Theoretical performance limits of multimode WGPDs.

On the basis of the above design procedure, we fabricated some prototype multimode WGPDs.[12] These WGPDs had a 0.6-μm-thick undoped InGaAs photo-absorption layer, and the total thickness of the InGaAs and InGaAsP layers was 1.8 μm. These were symmetric WGPDs with 4-μm-wide high-mesa structures. Using a hemispherically-ended single-mode fiber with a spot size of 1.3 μm, the external quantum efficiency η_{ex} was measured to be as high as 68% (If the AR-coating could be perfectly applied, the efficiency would have been 80%) and their 3-dB electrical frequency f_{3dB} was over 50 GHz, the upper detection limit of our measurement system (a 60-GHz-bandwidth was predicted by a SPICE simulation). Although a parasitic element ($R_S=35\,\Omega$) and an unexpectedly large inductance ($L_B=0.4$ nH) degraded the performance to some degree, the experimental value is very close to the calculated performance limit shown in Fig. 9.

3.3 Extended Design Concept to Overcome the $f_{3dB}\eta_{ex}$ Limit

Are there any ways of overcoming the performance limit of WGPDs? The degradation of the external quantum efficiency in the ultrawide-band region shown in Fig. 9 is mainly due to the coupling loss in the x direction, since a narrower photodetector width is required for a wider bandwidth. In order to overcome the $f_{3dB}\eta_{ex}$ limit, low loss coupling in the x direction is thus essential. To improve this coupling efficiency, we recently integrated a multimode WGPD with an input waveguide to compress the input light in the x direction through a tapered structure.[13]

This WGPD, shown in Fig. 10, was fabricated by two-step epitaxial growth. It has an asymmetric structure (0.6-μm undoped InGaAs/0.8-μm p^+-InGaAsP) and its tapered waveguide has a double-hetero structure (1-μm n-InP/0.1-μm n-InGaAsP/0.9-μm n-InP). The width of the input waveguide decreased from 4 μm to the width of the WGPD. The external quantum efficiency was measured and is plotted as a function of

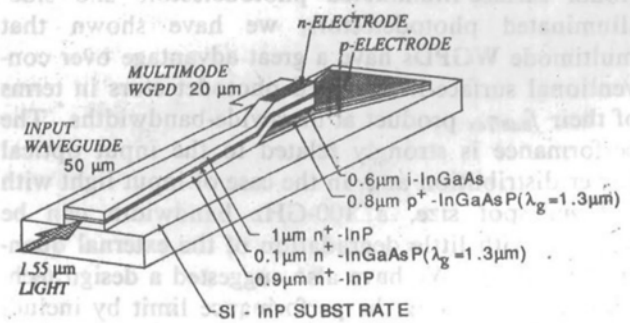

Fig. 10 Schematic view of the fabricated multimode WGPD with an input tapered waveguide.

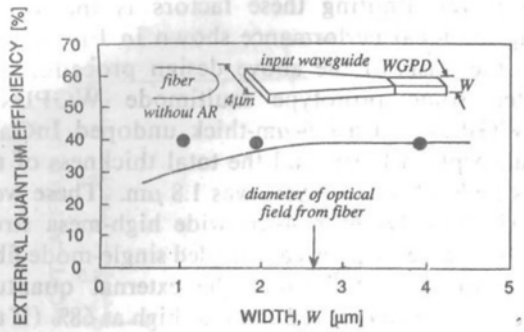

Fig. 11 Measured external quantum efficiency of the integrated WGPD (circles) and calculated efficiency of a solitary WGPD as a function of the WGPD width.

the WGPD width W as shown by the circles in Fig. 11. These results are compared with the calculated efficiency of a multimode WGPD without an input waveguide (shown by the curve). The external quantum efficiency (from the fiber to the WGPD via the waveguide) is almost independent of W and remains constant at 40% without an AR coating (more than 55% is expected with AR) even for a 1-μm-wide WGPD. The measured efficiency is mainly reduced by a radiation loss at the joint, but should be improved to be 80% (with AR) if a perfect butt-joint configuration can be achieved.

These results, together with the performance of the multimode WGPD discussed in the preceding sections, indicate that the dimensions of the photo-absorption layer can be reduced without degrading the coupling efficiency by means of a multimode waveguide structure for the y direction, and integration with a tapered waveguide for the x direction. This extended design concept should enable the performance limits of solitary multimode WGPDs to be overcome.

4. Conclusion

The tradeoff situation between the bandwidth and coupling efficiency of WGPDs can be resolved by adopting a multimode waveguide configuration. By calculating the performance limits of both conventional surface-illuminated photodetectors and side-illuminated photodetectors, we have shown that multimode WGPDs have a great advantage over conventional surface-illuminated photodetectors in terms of their $f_{3dB}\eta_{ex}$ product at ultrawide-bandwidths. The performance is strongly related to the input optical power distribution and, in the case of input light with a 1-μm spot size, a 100-GHz bandwidth can be achieved with little degradation of the external quantum efficiency. We have also suggested a design technique for increasing the performance limit by including an input tapered waveguide, and produced preliminary results which attest to the possibility of constructing limit-free photodetectors.

Acknowledgments

The authors would like to thank Mineo Ueki and Satoshi Oku for helping with the dry etching process, Dr. Kenji Sato for helping with the AR-coating process, and Drs. Junichi Yoshida and Haruhiko Tsuchiya for their encouragement.

References

(1) Bowers, J. E. and Burrus, C. A., "Ultrawide-band long-wavelength p-i-n photodetectors," *J. Lightwave Technol.*, vol. LT-5, pp. 1339-1350, Oct. 1987.
(2) Bowers, J. E. and Burrus, C. A., "High-speed zero-bias waveguide photodetectors," *Electron. Lett.*, vol. 22, pp. 905-906, Aug. 1986.
(3) Wake, D., Judge, S. N., Spooner, T. P., Harlow, M. J., Duncan, W. J., Henning, I. D. and O'Mahony, M. J., "Monolithic integration of 1.5 μm optical preamplifier and pin photodetector with a gain of 20 dB and a bandwidth of 35 GHz," *Electron. Lett.*, vol. 26, pp. 1166-1168, Jul. 1990.
(4) Kato, K., Hata, S., Kozen, A., Yoshida, J. and Kawano, K., "High-efficiency waveguide InGaAs pin photodiode with bandwidth of over 40 GHz," *IEEE Photon. Technol. Lett.*, vol. 3, pp. 473-474, May 1991.
(5) Wake, D., Spooner, T. P., Perrin, S. D. and Harlow, M. J., "50 GHz InGaAs edge-coupled pin photodetector," *Electron. Lett.*, vol. 27, pp. 1073-1075, Jun. 1991.
(6) Schlafer, J., Su, C. B., Powazinik, W. and Lauer, R. B., "20 GHz bandwidth InGaAs photodetector for long-wavelength microwave optical links," *Electron. Lett.*, vol. 21, pp. 496-471, May 1985.
(7) Lucovsky, G., Scharz, R. F. and Emmons, R. B., "Transit-time considerations in p-i-n diodes," *J. Appl. Phys.*, vol. 35, pp. 622-628, Mar. 1964.
(8) Wake, D., Blank, L. C., Walling, R. H. and Henning, I. D., "Top-illuminated InGaAs/InP p-i-n photodiodes with a 3-dB bandwidth in excess of 26 GHz," *IEEE Electron Device Lett*, vol. 9, pp. 226-228, May 1988.
(9) Kato, K., Hata, S., Kozen, A., Yoshida, J. and Kawano, K., "Highly efficient 40 GHz waveguide InGaAs p-i-n photodiode employing multimode waveguide structure," *IEEE Photon. Technol. Lett.*, vol. 3, pp. 820-822, Sep. 1991.
(10) Kawano, K., Wakita, K., Mitomi, O., Kotaka, I., Asai, H., Kawamura, Y. and Naganuma, M., "Design of InGaAs/InAlAs multiple quantum well (MQW) optical modulators," *IEEE J. Quantum Electron.*, vol. 28, pp. 224-230, Jan. 1992.
(11) Kawano, K., *Introduction and application of optical coupling system to optical devices*, Tokyo, Gendai-Kougakusha, 1991.
(12) Kato, K., Hata, S., Kawano, K., Yoshida, J. and Kozen, A., "A high-efficiency 50 GHz InGaAs multimode waveguide photodetector," in *IEEE J. Quantum Electron.*, Dec. 1992.
(13) Kato, K., Hata, S., Yoshida, J. and Kozen, A., "Design of a high-speed and high-sensitivity photodiode with an input optical waveguide on semi-insulating InP substrate," *Proc. 4th Int. Conf. on Indium Phosphide and Related Materials*, Newport, Rhode Island, 1992, paper WE4.

Kazutoshi Kato was born in Yokohama, Japan on January 29, 1961. He received the B.S. and M.S. degrees in physics from Waseda University, Tokyo, Japan, in 1985 and 1987, respectively. Since 1987 he has been working for NTT Opto-electronics Laboratories, Atsugi, Kanagawa, Japan, where he was engaged in research on receiver OEICs and high-speed photodetectors. He is a member of the Japan Society of Applied Physics, and IEEE.

Susumu Hata was born in Kagawa, Japan on December 8, 1947. He received the B.S. and M.S. degrees in electronic engineering from the Tokyo Institute of Technology, Tokyo, Japan, in 1970 and 1972, respectively. In 1972, he joined the Musashino Electrical Communication Laboratories, Nippon Telegraph and Telephone (NTT) Corporation, Tokyo, Japan, and engaged in research and development of semiconductor optical devices for optical communication systems. He is now with the NTT Opto-electronics Laboratories, Atsugi, Kanagawa, Japan. He is a member of the Japan Society of Applied Physics.

Kenji Kawano received the B.S. and M.S. degrees in physics and applied physics from Kyushu University, Fukuoka, Japan, in 1977 and 1979, respectively. He received the Ph.D. degree in 1989. He joined Musashino Electrical Communication Laboratories, Nippon Telegraph and Telephone (NTT) Corporation, Tokyo, Japan, in 1979, and was engaged in research on thin-film waveguides for microwave integrated circuits. Since 1982, his major efforts have been directed toward the research and development of optical devices for single-mode fiber transmission systems, with emphasis on semiconductor-laser-to-single-mode-fiber-coupling modules. Recently, his interest has been focused on the design and fabrication of $LiNbO_3$ high-speed optical waveguide modulators, multiple-quantum-well optical waveguide modulators and integrated semiconductor optical waveguide devices. He is an author of a book on coupling systems (Introduction and application of optical coupling systems to optical devices, Gendai Kougakusha, 1991). He is a senior research engineer, supervisor, at the NTT opto-electronics laboratories. Dr. Kawano is a member of the Japan Society of Applied Physics.

Atsuo Kozen was born in Tokyo, Japan on March, 7, 1954. He received the B.S. and M.S. degrees in applied chemistry from Waseda University, Tokyo, Japan, in 1976 and 1978, respectively. In 1978, he joined the Musashino Electrical Communication Laboratories, Nippon Telegraph and Telephone (NTT) Corporation, Tokyo, Japan, and was engaged in research on magnetic bubble materials. Since 1983, he has been engaged in research on MOVPE growth for opto-electronic devices. He is now with the NTT Opto-electronics Laboratories, Atsugi, Kanagawa, Japan. He is a member of the Japan Society of Applied Physics.